**Showcasing research from the Group of Prof. Shengjun Yuan at the Key Laboratory of Artificial Micro- and Nano-structures of Ministry of Education, School of Physics and Technology, Wuhan University, China.**

Strain-tunable magnetic and electronic properties of monolayer CrI$_3$

This work investigates the effect of strain on the electronic and magnetic properties of monolayer CrI$_3$, which undergoes a transition from a ferromagnetic state to an antiferromagnetic state. Moreover, a series of electronic phase transitions from magnetic-metal to half-metal to half-semiconductor to spin-relevant semiconductor is reported when biaxial strain varies from −15% to 10%. These results will help both theoretical and experimental researchers for further understanding the tunable electronic and magnetic properties of CrI$_3$ and its analogs.

ROYAL SOCIETY OF CHEMISTRY | Celebrating IYPT 2019

rsc.li/pccp

Check for updates
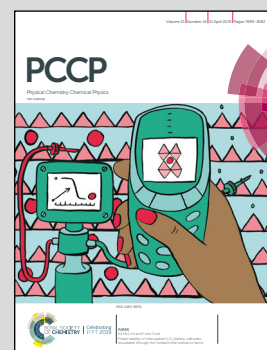
Strain-tunable magnetic and electronic properties of monolayer CrI₃†

Zewen Wu, [a] Jin Yu [*cb] and Shengjun Yuan [*ab]

Two-dimensional CrI$_3$ has attracted much attention as it is reported to be a ferromagnetic semiconductor with a Curie temperature of around 45 K. By performing first-principles calculations, we find that the magnetic ground state of CrI$_3$ is variable under biaxial strain. Our theoretical investigations show that the ground state of monolayer CrI$_3$ is ferromagnetic under compression, but becomes antiferromagnetic under tension. Particularly, the transition occurs under a feasible in-plane strain of around 1.8%. Accompanied by the transition of the magnetic ground state, CrI$_3$ undergoes a transition from magnetic-metal to half-metal to half-semiconductor to spin-relevant semiconductor when the strain varies from −15% to 10%. We attribute these transitions to the variation of the d-orbitals of Cr atoms and the p-orbitals of I atoms. Generally, we report a series of magnetic and electronic phase transitions in strained CrI$_3$, which will help both theoretical and experimental researchers in further understanding the tunable electronic and magnetic properties of CrI$_3$ and its analogs.

Introduction

Two-dimensional (2D) materials are of great concern theoretically and experimentally because of their unique electronic and optoelectronic properties.[1,2] Typically, graphene, which consists of six carbon atoms in a honeycomb lattice, is a zero-gap semimetal with the carrier mobility being reported up to $\sim 10^5 \text{ cm}^2 \text{ V}^{-1} \text{ s}^{-1}$.[3] When it is chemically decorated with added atoms or cut into 1D nanoribbons, it will exhibit tunable electronic and magnetic properties.[4–6] When combined with other 2D materials to form van der Waals (vdW) heterostructures,[7] it would exhibit much more interesting physical properties.[6,8] Besides graphene, other 2D materials from semiconducting black phosphorus[9] to transition metal dichalcogenides[10–12] to insulating hexagonal boron nitride[13] have also been identified as important candidates for the post-silicon electronic and optical devices.[14] However, none of them is reported to exhibit intrinsic magnetism, which limits their application in spintronics.[15] Theorists predicted that most 2D materials are nonmagnetic because the thermal fluctuations at finite temperature would break the spontaneous symmetry.[16] However, a composite of monolayer Cr$_2$Ge$_2$Te$_6$ has been reported to be ferromagnetic recently, which is regardless of the restriction.[17] The rise of Cr$_2$Ge$_2$Te$_6$ paves a new way to search for the long-range Ising ferromagnetism in atomically thin 2D

materials, where an intrinsic magnetocrystalline material could exist because of the reduction of the crystal symmetry.[18] Very recently, another ferromagnetic semiconductor chromium triiodide (CrI$_3$) appeared in the research field again[19] because of its high Curie temperature in the monolayer.[20] Upon carrier doping, room-temperature magnetism is observed in CrI$_3$ due to its flat band structure.[21–23] Both experimental and theoretical research shows that monolayer CrI$_3$ is a ferromagnetic semiconductor.[18,24] When increasing the number of layers, the ferromagnetic order persists within each layer, but the antiferromagnetic coupling dominates different layers.[8] Moreover, the ferromagnetic and antiferromagnetic states can be switched on and off by changing the external gate voltage.[18] When CrI$_3$ forms heterostructures with other 2D materials like graphene, it also exhibits some topological insulating properties.[25] However, all this is concluded from the fact that CrI$_3$ is a ferromagnetic semiconductor with an equilibrium lattice constant.[20]

On the other hand, strain plays an important role in determining the physical properties of 2D materials. Considering the fact that typically CrI$_3$ is transferred on the substrate of SiO$_2$ and on other 2D materials after exfoliation,[20] the intrinsic physical properties of CrI$_3$ would be affected by the substrate due to the lattice-mismatch-induced strain.[26,27] There are some studies on the physical properties of CrI$_3$ under strain, but they are based on the assumption of a robust ferromagnetic ground state.[28] Meanwhile, it is challenging for experimental researchers to identify the magnetic order of the monolayer in the atomic resolution. Here, we wish to identify the magnetic ground states of CrI$_3$ under strain *via ab initio* first-principles calculations.

a School of Physics and Technology, Wuhan University, Wuhan 430072, China
b Beijing Computational Science Research Center, Beijing 100094, China.
 E-mail: j.yu@science.ru.nl, s.yuan@whu.edu.cn
c Theory of Condensed Matter, Radboud University, Heyendaalseweg 135,
 6525 AJ Nijmegen, The Netherlands
† Electronic supplementary information (ESI) available. See DOI: 10.1039/c8cp07067a

In this work, we present a systematic study on the tunable electronic and magnetic properties of monolayer CrI_3 under strain. Our results show that the Cr atoms in the unit cell are ferromagnetically aligned under compression strain, and CrI_3 retains the magnetic order up to a maximum tension strain of around 2%, then it dramatically becomes an antiferromagnetic half-semiconductor when the tension strain is further increased. During this transition, the magnetic moment on Cr atoms increases, and CrI_3 undergoes a transition from magnetic-metal to half-metal to half-semiconductor, owing to the variation of the d-orbitals of Cr atoms and the p-orbitals of I atoms. Our results will provide a new way to understand the magnetic ground state in monolayer CrI_3 and its analogs, which is useful for the design of spintronic devices[29] based on ferromagnetic semiconductors.[17,30–32]

Results and discussion

The atomic structure of monolayer CrI_3 is shown in Fig. 1a, which can be simply imaged as a $\sqrt{3} \times \sqrt{3}$ super cell of 1T SnS_2 with one point vacancy of Sn atoms.[33–35] It belongs to space group $C2/m$ containing two formula units.[36] Its optimized lattice parameters are calculated to be $a = b = 6.978$ Å and $c = 21.476$ Å, which are in good agreement with the X-ray diffraction data[37] and previous DFT results.[24] Both spin-unpolarized and spin-polarized calculations are performed to get an overview of the ground state of monolayer CrI_3. Our result shows that the ferromagnetic (FM) state is more favorable in energy, which is 63 meV lower than the antiferromagnetic (AFM) state, indicating stable ferromagnetism at room-temperature. Thus, the intrinsic electronic and magnetic properties of CrI_3 can be represented by the FM state as shown in Fig. 1b and c. The spin-unpolarized band structure shows that nonmagnetic CrI_3 is a metal with several bands crossing through the Fermi level. Upon considering the spin-polarization, the degenerated bands get split, resulting in an indirect energy gap of 1.124 eV and 2.169 eV for the spin-up (solid) and -down (dashed) electrons, respectively. It is found that the spin-polarized

electrons in monolayer CrI_3 exhibit anisotropic transport properties. For the spin-up electrons, the conduction band minimum (CBM) and valence band maximum (VBM) are located at the Gamma point and in the line from gamma to M; for the spin-down electrons, the indirect gap originates from M and gamma points, respectively. It is also noted that the conduction and valence band edges around the Fermi level are fully spin-polarized and exclusively occupied by electrons with the same spin component, rendering a typical half-semiconductor character. Moreover, the CBM and VBM of the spin-up electrons are contributed by both Cr and I atoms, while the CBM and VBM of the spin-down electrons are contributed by Cr atoms and I atoms, respectively. Our conclusion of the intrinsic electronic structure of monolayer CrI_3 is further confirmed by the density of state (DOS) calculations, where sharp peaks composed of hybrid states appear around the Fermi level, suggesting strongly localized states. As a result, electrons are bound in these states and the carrier mobility of CrI_3 is very slow, which can be concluded directly from the nearly flat bands around the Fermi level. Thus, in some vdW heterostructures CrI_3 is usually used as a FM substrate to generate spin-polarized electrons.[7]

We have shown above that pristine CrI_3 is a ferromagnetic semiconductor with the magnetic moment on Cr atoms being 3.106 μ_B.[19,38] However, these 2D materials are usually supported by the substrate in device design. Besides the interlayer interaction, strain induced by lattice mismatch and lattice orientation is the most common case in these 2D materials. We noted in a very recent work that when a non-collinear spin configuration is introduced by considering the spin orbital coupling effect, monolayer CrI_3 will undergo a transition from the FM to AFM state under compression.[39] Here, we would like to show novel electronic and magnetic properties of monolayer CrI_3 under biaxial strain with a collinear spin configuration. The total energies are calculated using spin-polarized calculations for both FM and AFM configurations. It shows typically parabolic characters as in Fig. 2a when biaxial strain is applied. For the AFM configuration, its equilibrium lattice constant is slightly larger than that of the FM configuration. Under compression strain, the FM configuration prefers a much lower energy. To clearly show the variation of the total energy, we further plot the energy difference $\Delta E = E_{AFM} - E_{FM}$ as a function of biaxial strain in Fig. 2b, where E_{AFM} and E_{FM} are the total free energies of the monolayer with AFM and FM configurations, respectively. Within a reasonable range from -10% to 10%, ΔE decreases monotonously and drops down to zero around 1.8%, indicating a possible transition from FM to AFM. Taking the tensile strain of 3% as an example, the corresponding ΔE is 64 meV, which is twice larger than that calculated from the fluctuation of 300 K, suggesting stable AFM states at room temperature. When tension strain is further increased, the AFM configuration becomes much more stable. To confirm our conclusion, we performed further calculations with DFT+U, which usually give better results for transition metals with d orbitals.[40,41] The parameters J and U are chosen to be 0.7 eV and 2.7 eV, respectively, which have shown great success in predicting the magnetic anisotropic properties
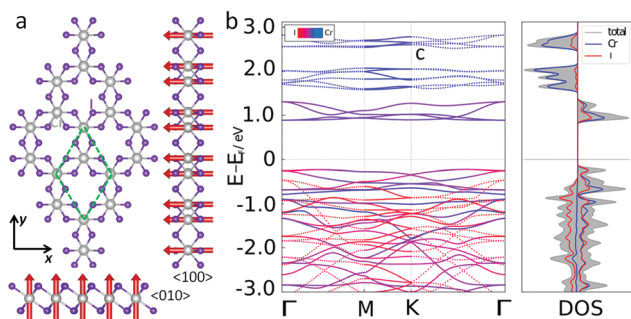

Fig. 1 Atomic and electronic structure of unstrained monolayer CrI_3. (a) Structural schematic of CrI_3 with top, front and right views. The green dashed line presents the unit cell and the red vectors indicate the spin configuration. (b) Band structure of ferromagnetic CrI_3. The Fermi level is set to zero, and the color indicates the attribution of Cr and I atoms. (c) Density of states of CrI_3 obtained by spin-polarized calculations.
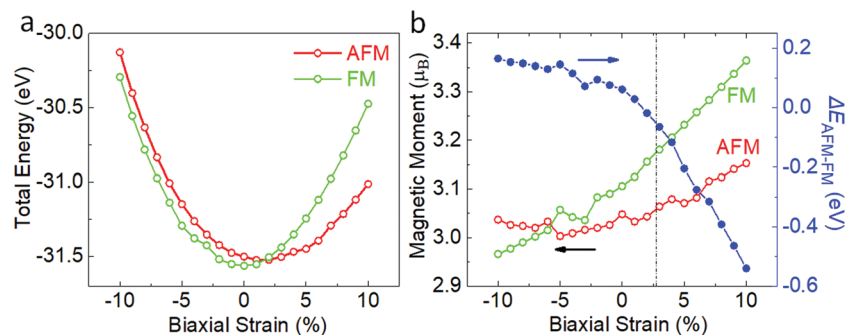
This journal is © the Owner Societies 2019

Phys. Chem. Chem. Phys., 2019, **21**, 7750–7755 | 7751

Fig. 2 Ground state of monolayer CrI_3 under biaxial strain. (a) Strain effect on the total energy of magnetic CrI_3. (b) Energy difference and magnetic moment of FM and AFM CrI_3 as a function of strain. Red and green symbols present the data of AFM and FM configurations, respectively.

of monolayer CrI_3.[39,42] We listed the total energies in Table S1 of the ESI.† One can clearly see that though the total energy of monolayer CrI_3 is higher than that of the standard DFT results, the relative variation trends of ΔE, E_{AFM} and E_{FM} are the same. As a result, the transition from the FM to AFM state occurs when the tension strain is applied.

AFM CrI_3 is reported to be stable under tensile strain in previous work, but their physical properties are less studied. The band structure of AFM CrI_3 plotted in Fig. 3 shows that tensed CrI_3 is an indirect gap spin-relevant semiconductor with the VBM and CBM at the K and M points, respectively. Different from that of the FM state, spin-polarized electrons degenerate in AFM CrI_3 as the inversion symmetry is preserved. As a result, spin-polarized electrons are strongly localized as seen from the nearly flat bands both around 1.0 and 2.0 eV, which disperse with an energy window of up to 0.5 eV in the FM configuration. The high degeneracy of the spin-polarized electrons is confirmed by the DOS as well, where the spin-up and -down electrons show identical distribution with mirror symmetry. Detailed analysis shows that though the contribution of the band structure is from the same atoms as FM CrI_3, the non-degenerated bands at some highly symmetric K points get split, indicating the symmetry breaking of the p_x and p_y orbitals in I atoms. It is also noted that when biaxial strain is applied, the magnetic moment on the Cr atoms can be tuned by biaxial strain. When in-plane strain is applied from the compression to the tension region, the magnetic moment on Cr atoms

increases for both FM and AFM configurations. Remarkably, the magnetic moment on the Cr atoms increases from 2.966 μ_B to 3.364 μ_B for FM CrI_3 when the strain varies from −10% to 10%. But the slope of the magnetic moment variation is much smaller in the AFM case.

In addition to the transition and modulation of the magnetic state, the electronic properties of CrI_3 show an interesting response to the external strain. We show the band gap of CrI_3 for both spin-up and -down electrons in Fig. 4. The left and right panels show the band gap modulation in the FM and AFM states, respectively. For the masked section, we will neglect the variation of the band gaps as the magnetic ground state has changed. It is obvious that the FM state is more sensitive to the biaxial strain as the slope of the modulated band gap is sharper than that of the AFM state. In the non-strained case (left panel), both spin-up and -down electrons open a gap showing the character of a half-semiconductor (HS); when a biaxial compression smaller than 13% is applied, the band gaps of both the spin-up and -down electrons decrease, as the band gap of spin-down electrons is larger than that of the spin-up electrons, at a critical value around 14%, the spin-up gap becomes zero, while the spin-down gap remains open with 0.103 eV, making CrI_3 a half-metal (HM); upon further compressing the monolayer, both the spin-up and -down bands close, and CrI_3 becomes a magnetic-metal (MM). In contrast, when tension strain is applied in a reasonable range (right panel), AFM CrI_3 shows spin-relevant semiconductor (SS) characters. Both spin-up and -down electrons occupy the same band and the band gap drops down in a slow slope around 0.015 eV/1%. Even when CrI_3 is stretched by 10%, it remains open with a large band gap of 1.189 eV, suggesting that CrI_3 is a robust AFM-SS when it is under tensile strain. The transition is further confirmed by our benchmark calculations of DFT+U as shown in Fig. S1 in the ESI.†

To understand the mechanism of the biaxial-strain-induced electronic phase transition from MM to HM to HS to SS, we examined the projected density of states (PDOS) of CrI_3 under various strains as shown in Fig. 5. Our result shows that the low-energy electronic properties of CrI_3 are mainly attributed to the in-plane components of the d orbitals of Cr atoms and the p orbitals of I atoms. And the p_x and p_y orbitals of I atoms are degenerated, which explains the degenerated VBs at some highly symmetric K points in FM CrI_3. On the other hand,
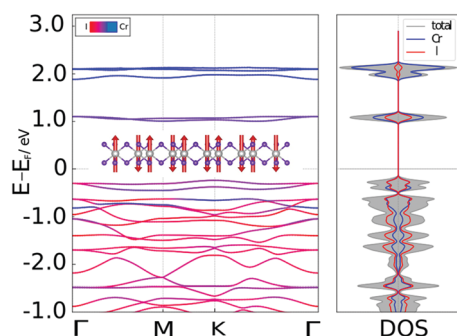

Fig. 3 Electronic structure of stretched CrI_3. Band structure and DOS of CrI_3 with a tension strain of 4%. The inset shows the spin configuration with the antiferromagnetic order. The Fermi level is set to zero.
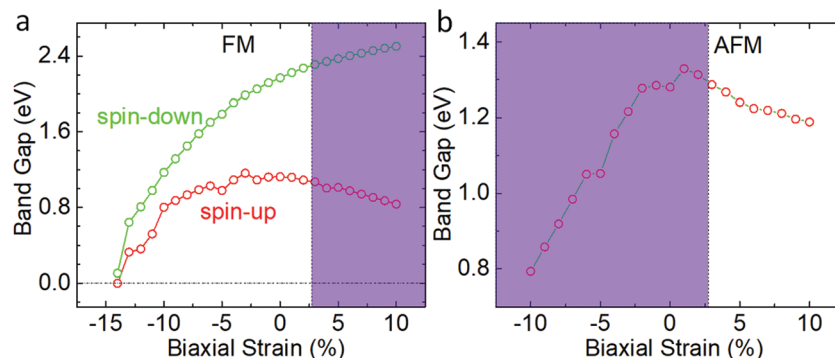
7752 | *Phys. Chem. Chem. Phys.*, 2019, **21**, 7750–7755

This journal is © the Owner Societies 2019

Fig. 4 Strain-dependent band gaps in CrI$_3$. (a and b) spin-relevant band gaps as a function of biaxial strain. Blue and green represent spin-up and -down electrons, respectively. The shadow indicates the artificial band gap modulation in the FM or AFM configuration.

the PDOS of Cr atoms is much higher than that of I atoms above the Fermi level, suggesting that the transport properties of electrons are dominated by the variation of the d-orbitals of Cr atoms, while the electronic properties of holes are determined by the p$_x$ and p$_y$ orbitals of I atoms. When the compression strain increases, the PDOS of all d-orbitals of Cr atoms shift downwards with a slightly decreasing gap for both the spin-up and spin-down electrons. However, the p$_x$ and p$_y$ orbitals of I atoms are much more sensitive to the biaxial strain, and the p orbitals at the conduction and valence region become hybridized, resulting in a closed gap. Specifically, at a compression strain state of −15%, all the d and p orbitals show peaks at the Fermi level; when the compression strain decreases to

−14%, only the p$_y$ orbitals of the spin-up electrons occupy the Fermi level, resulting in a MM–HM transition. For stretched CrI$_3$ with a tensile strain of 10%, the peaks of the PDOS from the p$_x$ orbital of I atoms are enhanced and the conduction region is contributed by two Cr atoms with mirror symmetry. We also show the spin density of CrI$_3$ at the bottom of Fig. 5. As the compression strain decreases from −15% to −10%, the spin density represented by the iso-surface increases slightly, which is in good agreement with the magnetic moment modulation in Fig. 2. To this end, we have shown that the electronic and magnetic properties of monolayer CrI$_3$ can be effectively tuned by biaxial strain, which is dominated by the d$_{xy}$, d$_{yz}$, d$_{z^2}$ and d$_{xz}$ orbitals of Cr atoms and the p$_x$ and p$_y$ orbitals of I atoms.
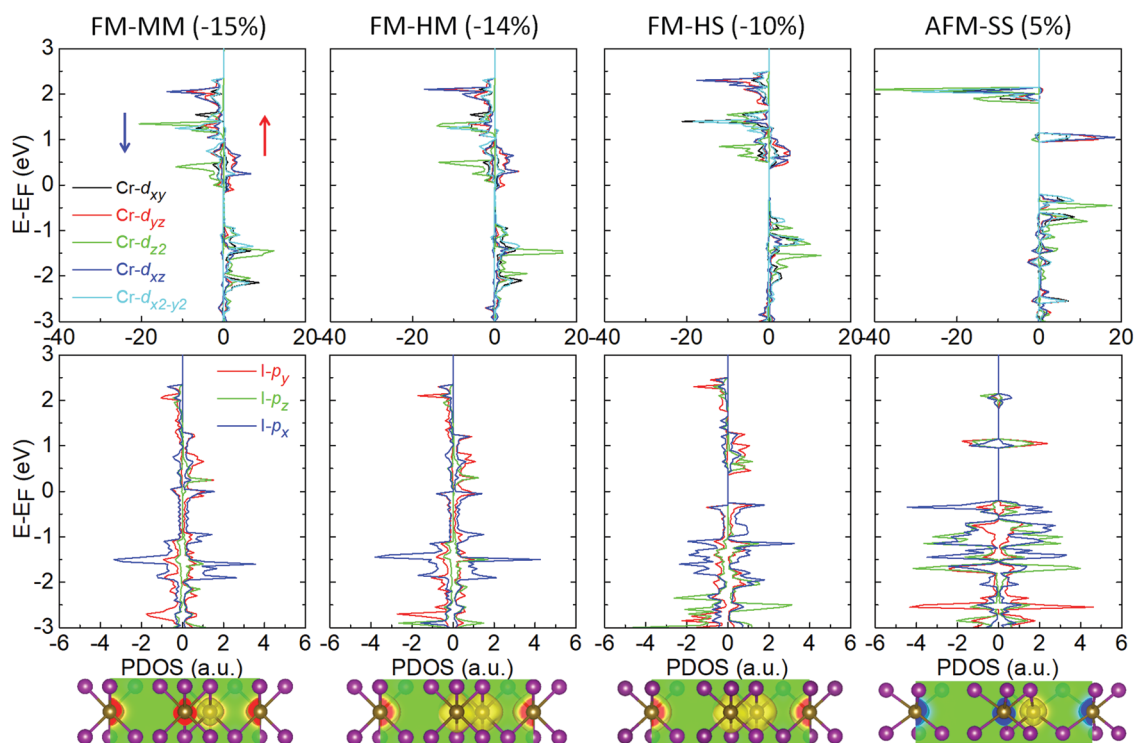

Fig. 5 Projected density of states and spin density at different strains for CrI$_3$ showing the MM–HM–HS transition. The scale bar in the slice of the spin density is set from −0.04 e Å^{-3} to 0.04 e Å^{-3}.

This journal is © the Owner Societies 2019

Phys. Chem. Chem. Phys., 2019, **21**, 7750–7755 | **7753**

Conclusions

In summary, we have systematically investigated the electronic and magnetic modulations of monolayer CrI_3 under biaxial strain by first-principles calculations. The applied strain yields a pronounced transition of the magnetic ground state between FM and AFM. When compression strain is applied, CrI_3 remains ferromagnetic. As the strain increases from −15% to 2%, a series of electronic phase transitions of MM–HM–HS–SS occur. In contrast, it becomes antiferromagnetic under tensile strain and the band gap of AFM CrI_3 is robust against external strain. These modulations of electronic and magnetic properties stem from the shift of the d-orbitals in Cr atoms and the p-orbitals in I atoms under strain. The tunable electronic and magnetic properties of monolayer CrI_3 investigated in this work are helpful in understanding the magnetism in CrI_3 and its analogs observed by experimental researchers and would inspire extensive research interest in modulation of the electronic and magnetic properties in ferromagnetic semiconductors.

Computational methods

All our simulations were carried out by performing spin-polarized density functional theory (DFT) calculations as implemented in the Vienna *ab initio* Simulation Package (VASP).[43] The Perdew–Burke–Ernzerhof (PBE) pseudopotentials[44] within the general gradient approximation (GGA)[45] were used to describe the electron exchange and correlation interactions and the energy cutoff was set at 520 eV. The Brillouin zone was represented by a $12 \times 12 \times 1$ mesh for geometry optimization and the total energy calculation. And for the DOS calculation, a much denser grid of $24 \times 24 \times 1$ was used. The atomic structure was fully relaxed with the energy convergence being 10^{-5} eV. To avoid the interlayer interaction between adjacent images, the vacuum was set to be 21 Å normal to the monolayer.

Conflicts of interest

There are no conflicts to declare.

Acknowledgements

References

1 A. K. Geim and K. S. Novoselov, The rise of graphene, *Nat. Mater.*, 2007, **6**(3), 183–191.

2 A. K. Geim, Graphene: Status and Prospects, *Science*, 2009, **324**, 1530–1534.

3 K. S. Novoselov, A. K. Geim, S. V. Morozov, D. Jiang, Y. Zhang, S. V. Dubonos, I. V. Grigorieva and A. A. Firsov, Electric Field Effect in Atomically Thin Carbon Films, *Science*, 2004, **306**, 666–669.

4 Y. W. Son, M. L. Cohen and S. G. Louie, Half-metallic graphene nanoribbons, *Nature*, 2006, **444**(7117), 347–349.

5 J. Yu and W. Guo, A New Paradigm to Half-Metallicity in Graphene Nanoribbons, *J. Phys. Lett.*, 2013, **4**(6), 951–955.

6 D. R. Klein, D. MacNeill, J. L. Lado, D. Soriano, E. Navarro-Moratalla, K. Watanabe, T. Taniguchi, S. Manni, P. Canfield, J. Fernández-Rossier and P. Jarillo-Herrero, Probing magnetism in 2D van der Waals crystalline insulators via electron tunneling, *Science*, 2018, **360**, 1218–1222.

7 D. Zhong, K. L. Seyler, X. Linpeng, R. Cheng, N. Sivadas, B. Huang, E. Schmidgall, T. Taniguchi, K. Watanabe, M. A. McGuire, W. Yao, D. Xiao, K.-M. C. Fu and X. Xu, van der Waals engineering of ferromagnetic semiconductor heterostructures for spin and valleytronics, *Sci. Adv.*, 2017, 3.

8 B. Huang, G. Clark, E. Navarro-Moratalla, D. R. Klein, R. Cheng, K. L. Seyler, D. Zhong, E. Schmidgall, M. A. McGuire, D. H. Cobden, W. Yao, D. Xiao, P. Jarillo-Herrero and X. Xu, Layer-dependent ferromagnetism in a van der Waals crystal down to the monolayer limit, *Nature*, 2017, **546**(7657), 270–273.

9 L. Li, Y. Yu, G. J. Ye, Q. Ge, X. Ou, H. Wu, D. Feng, X. H. Chen and Y. Zhang, Black phosphorus field-effect transistors, *Nat. Nanotechnol.*, 2014, **9**(5), 372–377.

10 Q. H. Wang, K. Kalantar-Zadeh, A. Kis, J. N. Coleman and M. S. Strano, Electronics and optoelectronics of two-dimensional transition metal dichalcogenides, *Nat. Nanotechnol.*, 2012, **7**, 699.

11 H. Zhong, R. Quhe, Y. Wang, Z. Ni, M. Ye, Z. Song, Y. Pan, J. Yang, L. Yang, M. Lei, J. Shi and J. Lu, Interfacial Properties of Monolayer and Bilayer MoS_2 Contacts with Metals: Beyond the Energy Band Calculations, *Sci. Rep.*, 2016, **6**, 21786.

12 J. He and S. Li, Two-dimensional Janus transition-metal dichalcogenides with intrinsic ferromagnetism and half-metallicity, *Comput. Mater. Sci.*, 2018, **152**, 151–157.

13 L. Song, L. Ci, H. Lu, P. B. Sorokin, C. Jin, J. Ni, A. G. Kvashnin, D. G. Kvashnin, J. Lou, B. I. Yakobson and P. M. Ajayan, Large Scale Growth and Characterization of Atomic Hexagonal Boron Nitride Layers, *Nano Lett.*, 2010, **10**(8), 3209–3215.

14 S. Z. Butler, S. M. Hollen, L. Cao, Y. Cui, J. A. Gupta, H. R. Gutiérrez, T. F. Heinz, S. S. Hong, J. Huang, A. F. Ismach, E. Johnston-Halperin, M. Kuno, V. V. Plashnitsa, R. D. Robinson, R. S. Ruoff, S. Salahuddin, J. Shan, L. Shi, M. G. Spencer, M. Terrones, W. Windl and J. E. Goldberger, Progress, Challenges, and Opportunities in Two-Dimensional Materials Beyond Graphene, *ACS Nano*, 2013, 7(4), 2898–2926.

15 Z. Li, T. Cao and S. G. Louie, Two-dimensional ferromagnetism in few-layer van der Waals crystals: renormalized spin-wave theory and calculations, *J. Magn. Magn. Mater.*, 2018, **463**, 28–35.

7754 | *Phys. Chem. Chem. Phys.*, 2019, **21**, 7750–7755

This journal is © the Owner Societies 2019

16 N. D. Mermin and H. Wagner, Absence of Ferromagnetism or Antiferromagnetism in One- or Two-Dimensional Isotropic Heisenberg Models, *Phys. Rev. Lett.*, 1966, **17**(22), 1133–1136.

17 D. Yang, W. Yao, Q. Chen, K. Peng, P. Jiang, X. Lu, C. Uher, T. Yang, G. Wang and X. Zhou, $Cr_2Ge_2Te_6$: High Thermoelectric Performance from Layered Structure with High Symmetry, *Chem. Mater.*, 2016, **28**(6), 1611–1615.

18 W.-B. Zhang, Q. Qu, P. Zhu and C.-H. Lam, Robust intrinsic ferromagnetism and half semiconductivity in stable two-dimensional single-layer chromium trihalides, *J. Mater. Chem. C*, 2015, **3**(48), 12457–12468.

19 J. F. D. Jr. and C. E. Olson, Magnetization, Resonance, and Optical Properties of the Ferromagnet CrI_3, *J. Appl. Phys.*, 1965, **36**(3), 1259–1260.

20 J. Liu, Q. Sun, Y. Kawazoe and P. Jena, Exfoliating biocompatible ferromagnetic Cr-trihalide monolayers, *Phys. Chem. Chem. Phys.*, 2016, **18**(13), 8777–8784.

21 H. Wang, F. Fan, S. Zhu and H. Wu, Doping enhanced ferromagnetism and induced half-metallicity in CrI_3 monolayer, *EPL*, 2016, **114**(4), 47001.

22 S. Jiang, L. Li, Z. Wang, K. F. Mak and J. Shan, Controlling magnetism in 2D CrI_3 by electrostatic doping, *Nat. Nanotechnol.*, 2018, **13**(7), 549–553.

23 L. Webster and J.-A. Yan, Strain-tunable magnetic anisotropy in monolayer $CrCl_3$, $CrBr_3$, and CrI_3, *Phys. Rev. B*, 2018, **98**(14), 144411.

24 H. Wang, V. Eyert and U. Schwingenschlogl, Electronic structure and magnetic ordering of the semiconducting chromium trihalides $CrCl_3$, $CrBr_3$, and CrI_3, *J. Phys.: Condens. Matter*, 2011, **23**(11), 116003.

25 Q. Tong, F. Liu, J. Xiao and W. Yao, Skyrmions in the Moiré of van der Waals 2D Magnets, *Nano Lett.*, 2018, **18**(11), 7194–7199.

26 J. Zhao, H. Liu, Z. Yu, R. Quhe, S. Zhou, Y. Wang, C. C. Liu, H. Zhong, N. Han, J. Lu, Y. Yao and K. Wu, Rise of silicene: a competitive 2D material, *Prog. Mater. Sci.*, 2016, **83**, 24–151.

27 X. Peng, Q. Wei and A. Copple, Strain-engineered direct-indirect band gap transition and its mechanism in two-dimensional phosphorene, *Phys. Rev. B: Condens. Matter Mater. Phys.*, 2014, **90**(8), 085402.

28 F. Zheng, J. Zhao, Z. Liu, M. Li, M. Zhou, S. Zhang and P. Zhang, Tunable spin states in the two-dimensional magnet CrI_3, *Nanoscale*, 2018, **10**(29), 14298–14303.

29 S. A. Wolf, D. D. Awschalom, R. A. Buhrman, J. M. Daughton, S. von Molnár, M. L. Roukes, A. Y. Chtchelkanova and D. M. Treger, Spintronics: A Spin-Based Electronics Vision for the Future, *Science*, 2001, **294**(5546), 1488.

30 W. Han, R. K. Kawakami, M. Gmitra and J. Fabian, Graphene spintronics, *Nat. Nanotechnol.*, 2014, **9**(10), 794–807.

31 P. Jiang, L. Li, Z. Liao, Y. X. Zhao and Z. Zhong, Spin Direction-Controlled Electronic Band Structure in Two-Dimensional Ferromagnetic CrI_3, *Nano Lett.*, 2018, **18**(6), 3844–3849.

32 V. Carteaux, D. Brunet, G. Ouvrard and G. Andre, Crystallographic, magnetic and electronic structures of a new layered ferromagnetic compound $Cr_2Ge_2Te_6$, *J. Phys.: Condens. Matter*, 1995, **7**(1), 69.

33 B. Qu, C. Ma, G. Ji, C. Xu, J. Xu, Y. S. Meng, T. Wang and J. Y. Lee, Layered SnS_2-Reduced Graphene Oxide Composite – A High-Capacity, High-Rate, and Long-Cycle Life Sodium-Ion Battery Anode Material, *Adv. Mater.*, 2014, **26**(23), 3854–3859.

34 J.-w. Seo, J.-t. Jang, S.-w. Park, C. Kim, B. Park and J. Cheon, Two-Dimensional SnS_2 Nanoplates with Extraordinary High Discharge Capacity for Lithium Ion Batteries, *Adv. Mater.*, 2008, **20**(22), 4269–4273.

35 J. Yu, E. van Veen, M. I. Katsnelson and S. J. Yuan, Effective lattice Hamiltonian for monolayer tin disulfide: tailoring electronic structure with electric and magnetic fields, *Phys. Rev. B*, 2018, **97**(24), 245410.

36 M. A. McGuire, H. Dixit, V. R. Cooper and B. C. Sales, Coupling of Crystal Structure and Magnetism in the Layered, Ferromagnetic Insulator CrI_3, *Chem. Mater.*, 2015, **27**(2), 612–620.

37 A. Frisk, L. B. Duffy, S. Zhang, G. van der Laan and T. Hesjedal, Magnetic X-ray spectroscopy of two-dimensional CrI_3 layers, *Mater. Lett.*, 2018, **232**, 5–7.

38 B. Rajeswaran, D. I. Khomskii, A. K. Zvezdin, C. N. R. Rao and A. Sundaresan, Field-induced polar order at the Néel temperature of chromium in rare-earth orthochromites: interplay of rare-earth and Cr magnetism, *Phys. Rev. B: Condens. Matter Mater. Phys.*, 2012, **86**(21), 214409.

39 L. Webster and J. A. Yan, Strain-tunable magnetic anisotropy in monolayer $CrCl_3$, $CrBr_3$, and CrI_3, *Phys. Rev. B*, 2018, **98**(14), 144411.

40 P. Guss, M. E. Foster, B. M. Wong, F. P. Doty, K. Shah, M. R. Squillante, U. Shirwadkar, R. Hawrami, J. Tower and D. Yuan, Results for aliovalent doping of $CeBr_3$ with Ca^{2+}, *J. Appl. Phys.*, 2014, **115**(3), 034908.

41 V. I. Anisimov, F. Aryasetiawan and A. I. Lichtenstein, First-principles calculations of the electronic structure and spectra of strongly correlated systems: the LDA+U method, *J. Phys.: Condens. Matter*, 1997, **9**(4), 767–808.

42 J. L. Lado and J. Fernandez-Rossier, On the origin of magnetic anisotropy in two dimensional CrI_3, *2D Mater.*, 2017, **4**, 3.

43 J. Hafner, *Ab-initio* simulations of materials using VASP: density-functional theory and beyond, *J. Comput. Chem.*, 2008, **29**(13), 2044–2078.

44 B. Hammer, L. B. Hansen and J. K. Nørskov, Improved adsorption energetics within density-functional theory using revised Perdew–Burke–Ernzerhof functionals, *Phys. Rev. B: Condens. Matter Mater. Phys.*, 1999, **59**(11), 7413–7421.

45 J. P. Perdew, K. Burke and M. Ernzerhof, Generalized Gradient Approximation Made Simple, *Phys. Rev. Lett.*, 1996, **77**(18), 3865–3868.